On the non-slip boundary condition enforcement in SPH methods.

Leo M. González
School of Naval Architecture ETSIN
Universidad Politécnica de Madrid
Madrid, Spain
leo.gonzalez@upm.es

A. Souto-Iglesias
School of Naval Architecture ETSIN
Universidad Politécnica de Madrid
Madrid, Spain
antonio.souto@upm.es

F. Macià
School of Naval Architecture ETSIN
Universidad Politécnica de Madrid
Madrid, Spain
fabricio.macia@upm.es

A. Colagrossi
The Italian Ship Model Basin
CNR-INSEAN
Roma, Italy
Centre of Excellence for Ship and Ocean Structures (CESOS)
NTNU
Trondheim, Norway
a.colagrossi@insean.it

M. Antuono
The Italian Ship Model Basin
CNR-INSEAN
Roma, Italy
matteoantuono@gmail.com

***Abstract*—The implementation of boundary conditions is one of the points where the SPH methodology still has some work to do. The aim of the present work is to provide an in-depth analysis of the most representative mirroring techniques used in SPH to enforce boundary conditions (BC) along solid profiles. We specifically refer to dummy particles, ghost particles, and Takeda *et al.* [1] boundary integrals. A Pouseuille flow has been used as a example to gradually evaluate the accuracy of the different implementations. Our goal is to test the behavior of the second-order differential operator with the proposed boundary extensions when the smoothing length h and other dicretization parameters as dx/h tend simultaneously to zero. First, using a smoothed continuous approximation of the unidirectional Pouseuille problem, the evolution of the velocity profile has been studied focusing on the values of the velocity and the viscous shear at the boundaries, where the exact solution should be approximated as h decreases. Second, to evaluate the impact of the discretization of the problem, an Eulerian SPH discrete version of the former problem has been implemented and similar results have been monitored. Finally, for the sake of completeness, a 2D Lagrangian SPH implementation of the problem has been also studied to compare the consequences of the particle movement.**

I. Introduction

The SPH simulations in Engineering involve usually solid boundary conditions (BC) for the velocity field and Dirichlet and Neumann type BC for other fields as, for instance, the temperature. In the SPH framework, these conditions are tackled in a number of ways: by using boundary forces-type models [2], [3] ; by modifying the structure of the kernel in the neighborhood of the boundaries [4]; by creating virtual particles inside the solid boundary domain through mirroring techniques. This latter approach is the main focus of the present work. An interesting study for the linear Couette and Pouseuille flows have been already performed in [5], but unfortunately the evolution of the kinetic energy was the only variable monitored in time.

In our case a well know problem as the Pouseuille flow will be used as a benchmark. The evolution of the velocity profile and the forces involved in the dynamics of the flow will be carefully studied.

II. Theoretical setup.

Before proceeding to the analysis, we briefly recall the principal results about the consistency of the continuous SPH formulation **without boundaries**. The fluid domain is $\Omega = \mathbb{R}^d$ and, therefore, its boundary is $\partial\Omega = \emptyset$.

Let $W(\mathbf{x}; h)$ be a function depending on $h > 0$ defined by

$$W(\mathbf{x}; h) := \frac{1}{h^d}\tilde{W}\left(\left|\frac{\mathbf{x}}{h}\right|\right), \tag{1}$$

We also define the function $F(r)$ as

$$F(r) := -\frac{1}{r}\tilde{W}'(r), \tag{2}$$

In the following we denote by $u(\mathbf{x})$ a smooth scalar field on $\mathbb{R}^d$.

For the approximation for the Laplacian of a function, the following formula due to Morris *et al.* [6] and Español *et al.* [7] is used:

$$\langle \Delta u \rangle_{\mathrm{M}}(\mathbf{x}) = 2\int_{\mathbb{R}^d} \frac{(\mathbf{x}' - \mathbf{x}) \cdot \nabla_{\mathbf{x}} W(\mathbf{x}' - \mathbf{x}; h)}{|\mathbf{x}' - \mathbf{x}|^2} \left[u(\mathbf{x}') - u(\mathbf{x})\right] d\mathbf{x}'. \tag{3}$$

As proved in [7], it follows:

$$\langle \Delta u \rangle_{\mathrm{M}}(\mathbf{x}) = \Delta u(\mathbf{x}) + \mathcal{O}(h^2). \tag{4}$$

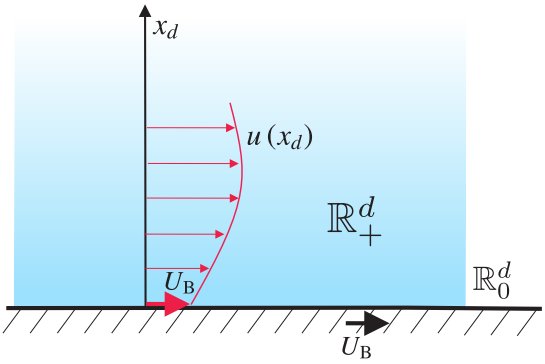

Fig. 1. Unidirectional vector field

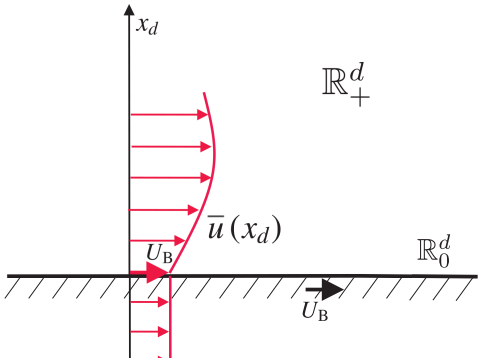

Fig. 2. Constant extension U0M

Again, note that no *a priori* assumptions on the smoothness of u have to be made in order to define $\langle \Delta u \rangle_{\mathrm{M}}$.

III. Boundary conditions

The most representative mirroring techniques in SPH to impose non-slip boundary conditions are: rows of fixed (boundary velocity) dummy particles (U0M) [8], ghost particles with antisymmetric mirroring (ASM) [9], [10] and the Takeda *et al.* [1] imaginary particles.

For the sake of simplicity, we consider unidirectional velocity fields $\mathbf{u}\,(\mathbf{x})$ defined in the upper-half plane

$$\mathbb{R}^d_+ := \left\{ (\mathbf{x}', x_d) \in \mathbb{R}^d : x_d > 0 \right\},$$

that are infinitely differentiable and that satisfy a non-slip boundary condition on

$$\mathbb{R}^d_0 := \partial \mathbb{R}^d_+ = \left\{ (\mathbf{x}', 0) : \mathbf{x}' \in \mathbb{R}^{d-1} \right\}.$$

A regular solid surface can be approximated with its tangent plane in the neighborhood of the fluid particle for $h \ll 1$. In this framework, the tangent plane can be identified with $x_d = 0$.

This class of velocity fields appear in a number of canonical problems in different physical contexts as, for instance, unidirectional incompressible fluid flow (Couette, plane Poiseuille, etc.). Note that heat conduction problems also fit this framework by replacing the velocity with the temperature field.

In general, such a velocity field takes the following form (see figure (1)):

$$\mathbf{u}\,(\mathbf{x}) := (u\,(x_d), 0, ..., 0)\,. \tag{5}$$

We assume that $\mathbf{u}\,(\mathbf{x})$ satisfies the boundary condition:

$$\mathbf{u}\,(\mathbf{x}', 0) = (u\,(0), 0, ..., 0) = (U_{\mathrm{B}}, 0, ..., 0)\,,$$

where U_{B} is the boundary velocity magnitude and, close to the boundary inside the fluid domain, the component u takes the form:

$$u\,(x_d) = U_{\mathrm{B}} + a_1 x_d + a_2 x_d^2 + ...\tag{6}$$

The mirroring techniques we deal with produce an extension $\overline{\mathbf{u}}\,(\mathbf{x})$ of the velocity field $\mathbf{u}\,(\mathbf{x})$ to the whole space $\mathbb{R}^d$. Here, we analyze the action of the continuous SPH approximation of the Laplacian operator on these mirrored (extended) velocity fields. Due to the specific form of the velocity fields, this corresponds to an extension of the scalar function $u\,(x_d)$, defined only of the half axis $x_d \geq 0$, to a function $\overline{u}\,(x_d)$ defined on the whole real line $\mathbb{R}$.

The SPH approximations to the Laplacian of $\overline{u}$, $\langle \Delta \overline{u} \rangle_{\mathrm{M}}$ are of the same order of differentiability of $\overline{u}$.

Finally, we introduce the following h-independent constants that will appear repeatedly in the rest of the article:

$$M_0 := \int_{\mathbb{R}^d} F\,(|\mathbf{y}|)\,d\mathbf{y}, \tag{7}$$

$$M_1 := \int_{\mathbb{R}^d_+} y_d F\,(|\mathbf{y}|)\,d\mathbf{y}, \tag{8}$$

$$C_p := \int_{\mathbb{R}^d} |y_d|^p\, \tilde{W}\,(|\mathbf{y}|)\,d\mathbf{y}, \tag{9}$$

Note that $C_0 = 1$, $M_0 = 2$ and $M_1 = 1/\sqrt{\pi}$.

Let us consider a general polynomial profile $u\,(\mathbf{x}) = U_{\mathrm{B}} + x_d^p$ with $p \geq 1$ for the calculations performed in section III.

A. Constant extension (U0M)

Define the constant extension of u as (see Figure 2):

$$\overline{u}\,(\mathbf{x}) := \begin{cases} u\,(\mathbf{x}) & x_d > 0, \\ U_{\mathrm{B}} & x_d \leq 0. \end{cases}$$

This technique is usually referred to as the Dummy Particles (DP) method. It is simple to implement and has been used, for instance, by Monaghan [8] for modeling a transient Couette flow.

Since the function $u\,(\mathbf{x})$ only depends on x_d, we obtain the following expression for the boundary values of the SPH Laplacian approximation:

$$\langle \Delta \overline{u} \rangle_{\mathrm{M}}\,(\mathbf{x}', 0) = \frac{2}{h^2}\left[\int_{\mathbb{R}^d_+} u\,(h y_d)\, F\,(|\mathbf{y}|)\,d\mathbf{y} - U_{\mathrm{B}} \frac{M_0}{2} \right] =$$

$$= \begin{cases} \dfrac{2M_1}{h}, & \text{for } p = 1, \\ 1, & \text{for } p = 2 \\ h^{p-2}\,(p-1)\,C_{p-2}, & \text{for } p > 2. \end{cases}, \tag{10}$$

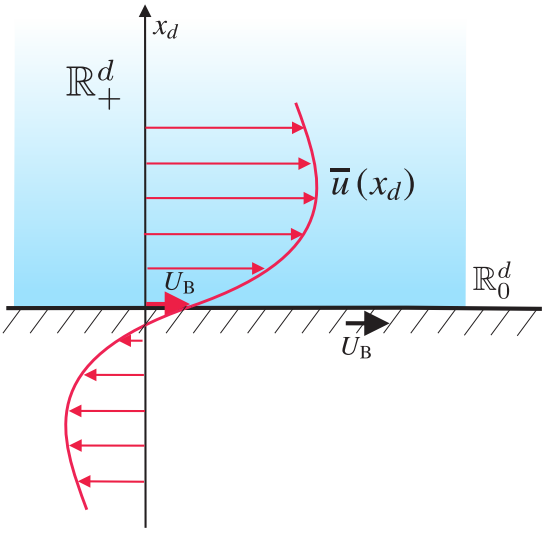

Fig. 3. Antisymmetric extension ASM

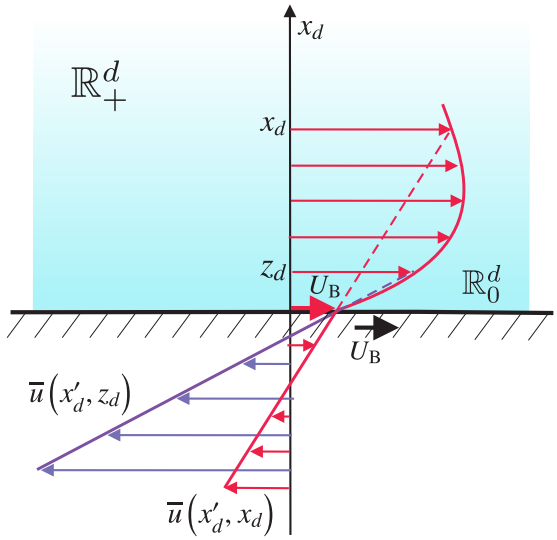

Fig. 4. Takeda *et al.* [1] extension

For details of the derivation of the equation 10, see [11].

B. Antisymmetric extension (ASM)

Next we consider the antisymmetric extension of u defined as (see Figure 3):

$$\overline{u}(\mathbf{x}) := \begin{cases} u(\mathbf{x}) & x_d > 0, \\ 2U_B - u(\mathbf{x}', -x_d) & x_d \leq 0. \end{cases}$$

This is the most widespread method to implement the solid BC. In the SPH literature it is generally referred to as the ghost particles (GP) method (e.g. [9], [10], [12]).

The expression for the Laplacian is:

$$\langle \Delta \overline{u} \rangle_M (\mathbf{x}', 0) = 0. \tag{11}$$

We again refer to [11] for a justification of these results.

C. Takeda et al. [1] extension

We define the Takeda *et al.* [1] extension of a function $u(x_d)$ by:

$$\overline{u}(x'_d, x_d) := \begin{cases} u(x'_d) & x'_d > 0, \\ (u(x_d) - U_B)\dfrac{x'_d}{x_d} + U_B & x'_d \leq 0, \end{cases}$$

where $x_d > 0$ and $x'_d \in \mathbb{R}$. Note that this extension procedure is slightly different from those previously discussed. Indeed, it associates to each point x_d in the fluid domain an extended field $\overline{u}(x'_d, x_d)$ defined for $x'_d \in \mathbb{R}$ and the extension actually depends on the point x_d. Figure 4 provides an illustration of this procedure.

As done before, let $u(x_d) = x_d^p + U_B$ with $p \geq 1$. Clearly, we have:

$$\overline{u}(x'_d, x_d) := \begin{cases} (x'_d)^p + U_B & x'_d > 0, \\ x_d^{p-1} x'_d + U_B & x'_d \leq 0. \end{cases}$$

Note that for $p = 1$, we have $\overline{u}(x'_d, x_d) = x'_d + U_B$. Concerning the Laplacian, we obtain:

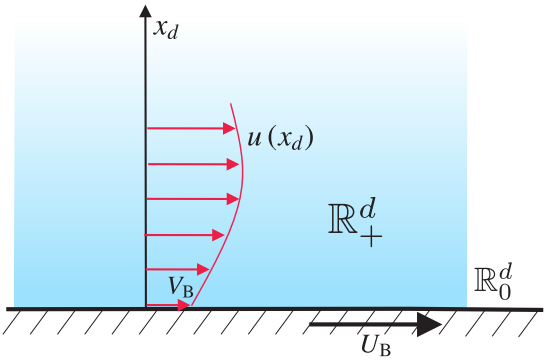

Fig. 5. Velocity field not satisfying the boundary condition U_B

$$\langle \Delta \overline{u} \rangle_M (\mathbf{x}', 0) = 2h^{p-2} \int_{\mathbb{R}^d_+} y_d^p F(|\mathbf{y}|)\, d\mathbf{y} =$$

$$= \begin{cases} 0 & \text{for } p = 1, \\ h^{p-2}(p-1) C_{p-2} & \text{for } p > 1, \end{cases} \tag{12}$$

D. Flows not satisfying the boundary condition

In this section we shall consider again velocity fields of the form (5) but we shall not assume that the value of $u(x_d)$ as x_d approaches the boundary $x_d = 0$ coincides with the boundary value U_B (see Figure 5). These velocity fields appear as initial values in a number of viscous flows, as for instance unsteady Couette flow, plane semi-infinite plate flow or, more generally, free shear layer flows [13].

Let us denote by V_B the value of $u(x_d)$ for $x_d \to 0^+$; we are assuming that $U_B \neq V_B$. One remark should be done:

1) *The Takeda et al. [1] extension produces a singular function, that is not even well-defined at* $x_d = 0$. The

extended field equals in this case

$$\overline{u}\left(x'_d, x_d\right) := \begin{cases} \left(x'_d\right)^p + V_{\mathrm{B}} & x'_d > 0, \\ x_d^{p-1} x'_d + \left(V_{\mathrm{B}} - U_{\mathrm{B}}\right) \dfrac{x'_d}{x_d} + U_{\mathrm{B}} & x'_d \leq 0, \end{cases} \tag{13}$$

which clearly has not a definite value at $x_d = 0$. Therefore, the Takeda et al. [1] extension does not seem to be suitable to deal with discontinuous extensions.

The remaining mirroring techniques we have dealt with so far will produce an extended field $\overline{u}$ presenting a discontinuity at $x_d = 0$. Therefore, the behavior of the continuous SPH approximations of differential operators acting on these extended fields will present singularities on $x_d = 0$ of higher order than those already described for the case $U_{\mathrm{B}} = V_{\mathrm{B}}$.

As previously discussed, the singularities induced by the U0M and ASM models are stronger when the field does not satisfy the boundary condition. We illustrate this by analyzing the U0M model, the results for the ASM model are rather similar. Consider the field $u\left(x_d\right) = V_{\mathrm{B}} + x_d^p$ for $p \geq 1$; $\overline{u}$ will denote its extension by U_{B} for $x_d < 0$. The Laplacian gives:

$$\langle \Delta \overline{u} \rangle_{\mathrm{M}} \left(\mathbf{x}', 0\right) = h^{p-2} p C_{p-1} + \frac{V_{\mathrm{B}} - U_{\mathrm{B}}}{h^2} M_0. \tag{14}$$

We therefore see that the boundary value of the derivative behaves as $1/h$ whereas that of the Laplacian is more singular, behaving as $1/h^2$.

In conclusion, none of the mirroring techniques discussed here is suitable to deal directly with velocity fields that do not satisfy the boundary condition exactly. This difficulties can be overcome by suitably modifying the velocity field in the neighborhood of the boundary in order to perform a continuous matching with the boundary value U_{B}. The exact nature of these modifications will be the subject of future work.

IV. Results

A time dependant plane Poiseuille flow can be described in $\mathbb{R}^2$ by the mathematical expression, see [13]:

$$\rho \frac{\partial u(x_2, t)}{\partial t} = -\nabla P + \mu \Delta u(x_2, t) \tag{15}$$

where ρ and μ are the fluid density and viscosity respectively, u is the first component of the unidirectional velocity field $\mathbf{u} = (u, 0)$ and ∇P is a constant pressure gradient that drives the flow between the two parallel plates towards the increasing x_1 values. The parallel plates will be set at $x_2 = 0$ and $x_2 = 1$ consequently the boundary conditions can be expressed as:

$$\begin{aligned} u(0) &= 0 \\ u(1) &= 0 \end{aligned}$$

The solution to this problem is a superposition of a linear velocity field ($p = 1$) plus a quadratic velocity field ($p = 2$), this is:

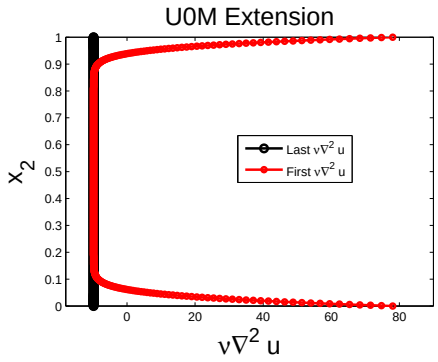

Fig. 6. Snapshots of $\nu \Delta u$ at the first and the last(stationary stage) time step.$h = 1/15$

$$u(x_2) = \frac{-\nabla P}{2\mu} x_2 (1 - x_2) \tag{16}$$

The Pouseuille flow is a sufficient paradigmatic example that presents most of the inconsistencies detected in the formulation described before when (16) is introduced as initial condition.

The equivalent expression to the equation (18) for a SPH particle, where the vertical velocity component is zero, see [12] is:

$$\frac{du_a}{dt} = -\nabla P_a + \mathbf{\Pi}_a \tag{17}$$

where the subscript a refers to the particle that carries over the considered property and $\mathbf{\Pi}_a$ represents the viscous interaction. The kernel used in the discretized SPH simulations is the normalized Gaussian kernel with support $3h$ [14], where h is the smoothing length.

To quantify the viscous interaction the Morris viscosity model (MVT) was used [6]. The stopping criteria used to quit the simulation was:

$$\max_i \{\mu \Delta u_i^k - \nabla P\} \leq 10^{-1} \tag{18}$$

where u_i^k is the velocity value of the fluid particle i at the time step k. The steady state is reached when the pressure gradient is balanced with the viscous force for all fluid particles.

The initial velocity used for the for the fluid particles is equal to the exact analytical solution $u^0(x_2) = -\frac{\nabla p}{2\mu} x_2 (1 - x_2)$, the pressure gradient has been fixed to $\nabla P = -9.8$, $\mu = 0.744$ and $\rho = 1$ for all simulations.

V. 1D Continuous time dependant Pouseuille flow.

The equation (18) has been discretized in time by an Euler time scheme, while the Laplacian operator has not been discretized and the integrals coming from this part have been accurately calculated by Matlab. The spatial domain considered is $x_2 \in \mathbf{R}$. In this context the (continuous) solution of the Pouseuille flow should be recovered as h tends to zero.

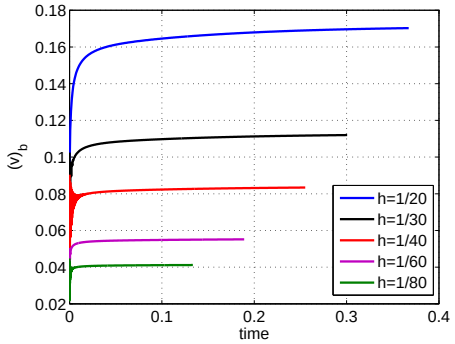

Fig. 7. Evolution of the velocity at the boundaries for different h values.

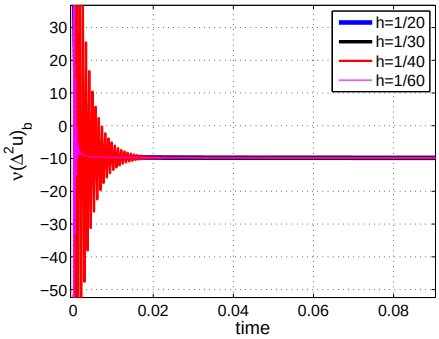

Fig. 8. Evolution of the $\mu\Delta^2 u$ at the boundaries for different h values. The asymptotic value tends to $\nabla P = -9.8$ when $h \to 0$

At the first time step, when the Laplacian of the initial condition is calculated with the U0M extension the result presents a erroneous values in a boundary layer close to the plates, see the red curve in figure 6. This incorrect tendency of the viscous force calculated at the boundaries has been already predicted as $1/h$ in section II. It has opposite sign to the expected correct value (order ∇P), consequently it acts as a boundary driving force that helps the pressure gradient to increase the velocity of the particles closest to the boundaries. Using the results obtained in section II, we can calculate the slip velocity at the boundary v_b^1 after the first iteration:

$$v_b^1 = \Delta t(-\nabla P + \mu\nabla^2(\frac{-\nabla P}{2\mu}(x_2 - x_2^2))) = \quad (19)$$

$$\Delta t(-\nabla P + (\frac{-\nabla P}{2}(\nabla^2 x_2 - \nabla^2 x_2^2))) = \quad (20)$$

$$\Delta t(-\nabla P + (\frac{-\nabla P}{2}(\frac{2M_1}{h} - 1))) = \quad (21)$$

$$-\Delta t\nabla P(\frac{M_1}{h} + \frac{1}{2}) \quad (22)$$

This velocity perturbs the initial condition (analytic solution) on the boundary as $1/h$. The velocity v^1 could be decomposed in two parts, a constant profile v_b^1 plus another profile v_{nb}^1 that satisfies the boundary condition, as $v^1 = v_b^1 + v_{nb}^1$. The Laplacian of v^1 will have two contributions at the boundary:

$$\mu\nabla^2 v_b^1 = \mu\nabla^2 v_b^1 + \mu\nabla^2 v_{nb}^1 = \quad (23)$$

$$-\mu\frac{M_0 v_b^1}{h^2} + O(\frac{\nabla P}{2}) + O(-\nabla P\frac{M_1}{h}) \quad (24)$$

The momentum equation can be written as:

$$\frac{dv_b}{dt} = -\mu\frac{M_0 v_b^1}{h^2} + O(\frac{\nabla P}{2}) + O(-\nabla P\frac{M_1}{h}) - \nabla P \quad (25)$$

We can observe in equation (25), that the term $-\mu\frac{M_0 v_b^1}{h^2}$ plus $O(\frac{\nabla P}{2})$ create a friction force that works against the pressure gradient $-\nabla P$ and the third term $O(-\nabla P\frac{M_1}{h})$. In our simulation the driving forces (pressure gradient plus third term) are bigger than the friction terms, creating a positive acceleration at the boundary. This acceleration increases the slip velocity v_b, but this effect increases also the first term. There is an instant $t = t_n$ where the equilibrium between the driving and the friction forces is obtained and the friction coming from the slip velocity is able to equilibrate the driving terms. The residual velocity in that instant can be estimated as:

$$\mu\frac{M_0 v_b^n}{h^2} \sim O(\frac{-\nabla P}{2}) + O(-\nabla P\frac{M_1}{h}) \quad (26)$$

then,

$$v_b^{n+1} \sim O(h) + O(h^2) \quad (27)$$

Looking at figure 7 we can see the boundary velocity evolution from the first initial value towards the stationary value for different values of the smoothing kernel h. This tendency is basically produced by the presence of the term $-\mu\frac{M_0 v_b^1}{h^2}$ which creates a large deceleration of the boundary fluid when h is small enough. Similarly, the evolution of the viscous force $\mu\Delta u$ at the boundary has been plotted for different h values, see figure 8. From figure 8 we can appreciate that all curves start in $\frac{-\nabla P}{2}(\frac{2M_1}{h} - 1)$ and tend to the value $\nabla P = -9.8$ that balances the pressure gradient and takes the problem to the stationary state.

The absolute errors in the stationary solution compared to the exact solution for the whole fluid have been plotted in figure 9, where we can clearly appreciate that the error decreases when h tends to zero.

To test the result obtained in the equation (27), the residual slip velocities have been approximated by a second order polynomial $v_{slip} = ah^2 + bh$, as we can observe in figure 10 a second order polynomial fits the computational values obtained accurately and shows that the residual slip velocity tends to zero consistently when the smoothing length decreases.

The absolute error of the stationary velocity profile compared to the exact solution is plotted in 9 for different h values.

When a different extension ASM is used in order to impose the boundary conditions, the Laplacian of the initial condition

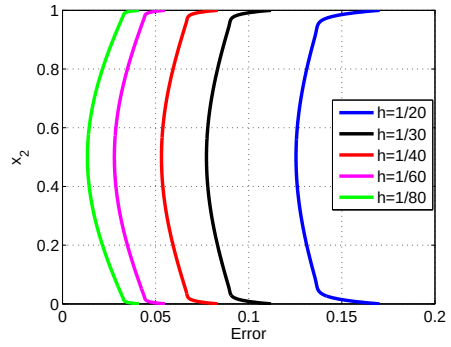

Fig. 9. Absolute error of the stationary velocity field compared with the analytical solution for different values of the parameter h when the U0M extension is used.

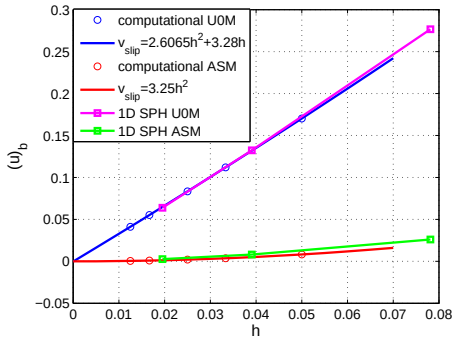

Fig. 10. Dependence on h and h^2 of the slip boundary velocity.

gives a erroneous zero value close to the boundary, see figure 11. Consequently, at this point, viscous friction does not equilibrate the pressure gradient and increases the velocity of the closest particles to the boundaries producing a slip velocity v_b^1.

$$v_b^1 = \Delta t(-\nabla P + (\frac{-\nabla P}{2}(\nabla^2 x_2 - \nabla^2 x_2^2))) = -\Delta t \nabla P \quad (28)$$

Due to the absence of friction at the boundaries, the initial

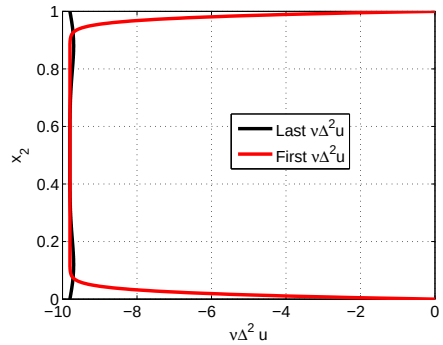

Fig. 11. Snapshots of $\nu\Delta u$ at the first and the last (stationary stage) time step when the U0M extension is used.$h = 1/20$

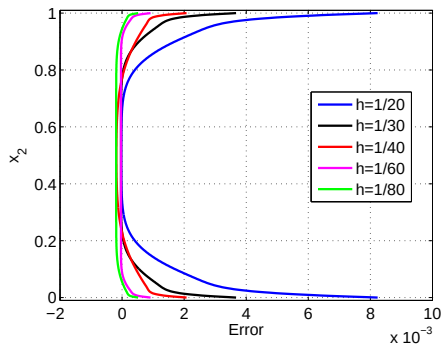

Fig. 12. Absolute error of the stationary velocity field compared with the analytical solution when the U0M extension is used.

condition (analytic solution) is locally perturbed. As in the U0M case, the velocity v^1 could be decomposed in two parts, a constant profile v_b^1 plus another profile v_{nb}^1 that satisfies the boundary condition, as $v^1 = v_b^1 + v_{nb}^1$. The Laplacian of such velocity will have two contributions at the boundary:

$$\mu\nabla^2 v^1 = \mu\nabla^2 v_b^1 + \mu\nabla^2 v_{nb}^1 = -\mu\frac{2M_0 v_b^1}{h^2} \quad (29)$$

The resulting momentum equation can be written as:

$$\frac{dv_b^2}{dt} = -\nabla P - \mu\frac{2M_0 v_b^1}{h^2} \quad (30)$$

The second friction term $-\mu\frac{M_0 v_b^1}{h^2}$ works against the pressure gradient. At the beginning of our simulation the driving pressure gradient is bigger than the friction term, creating an acceleration at the boundary. This acceleration increases the slip velocity v_b and consequently the friction term also grows. There is an instant $t = t_n$ where the equilibrium is obtained and the friction coming from the slip velocity is able to equilibrate the pressure gradient. The residual boundary velocity can be calculated as:

$$\mu\frac{2M_0 v_b^n}{h^2} = -\nabla P \quad (31)$$

Then, the residual slip velocity will be:

$$v_b^n = \frac{-\nabla P}{2M_0\mu}h^2 \quad (32)$$

The coefficient $\frac{-\nabla P}{2M_0\mu}$ in our case is equal to 3.25 which is equal to the coefficient of the interpolation expression used in figure 10. This means than the theoretical prediction shown in equation 32 agrees perfectly with the computational results.

In figure 13 the evolution of the residual boundary velocity has been plotted. We can observe that the asymptotic final value is the result of the two opposite forces (viscous friction $-\mu\frac{2M_0 v_b^1}{h^2}$ and pressure gradient) that work against each other until they reach the final stationary state. The consistency of

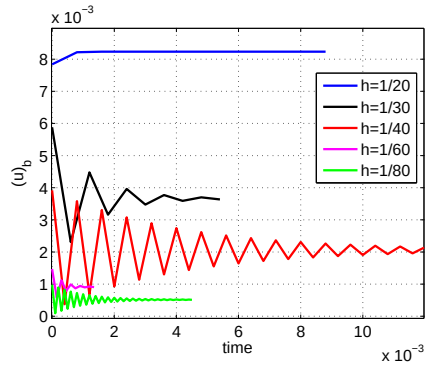

Fig. 13. Evolution of the velocity at the boundaries for different h values when the ASM extension is used.

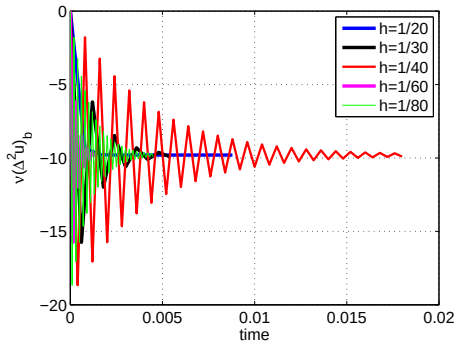

Fig. 14. Evolution of the $\mu\Delta^2 u$ at the boundaries for different h values when the ASM extension is used.

this residual velocity is guaranteed by the fact that its final value tends to zero when the smoothing length h decreases. A complementary result is shown in figure 14 where μ times the Laplacian of the velocity calculated at the boundary is initially equal to $\frac{-\nabla P}{2}(\frac{2M_1}{h}-1)$.

When the Takeda extension is used, just the first time step can be calculated with this continuous methodology. When the Laplacian of the initial condition is calculated with the Takeda extension the result gives a erroneous halved value in a boundary layer of size h. This wrong friction at the boundaries does not equilibrate the pressure gradient and consequently the velocity of the closest particles to the boundaries increases producing a slip velocity v_b^1.

$$v_b^1 = \Delta t(-\nabla P + \mu\nabla^2(\frac{-\nabla P}{2\mu}(x_2 - x_2^2))) = \quad (33)$$

$$\Delta t(-\nabla P + (\frac{-\nabla P}{2}(\nabla^2 x_2 - \nabla^2 x_2^2))) = \quad (34)$$

$$-\Delta t\frac{\nabla P}{2} \quad (35)$$

As we know from section II, the existence of a slip velocity that does not satisfy the boundary condition makes the Takeda extension produce a singular function, that is not even well-defined at the boundaries. The extended field has not a definite value at $x_2 = 0$ and $x_2 = 1$. Therefore, the Takeda extension

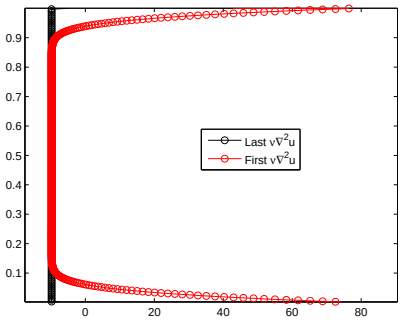

Fig. 15. Snapshots of $\nu\Delta u$ calculated with the 1D Eulerian discrete approximation at the first and the last(stationary stage) time step using the U0M extension. $h = 1/15$ and $h/dx = 512/15$.

cannot be studied with this continuous algorithm and its study will be postponed to further discrete approximations.

Finally a re-normalized Takeda extension, see [11], has also been tested. The viscous friction at the first iteration is calculated exactly $\mu\Delta^2 u^0 = \nabla P$ and consequently the stationary condition is satisfied $u^n = u^0$.

VI. 1D Discrete approximation

In this section, the scheme used to solve the Pouseuille problem will be a Eulerian approximation where a column of particles remains in fixed positions. Comparing this procedure with the one presented in section V, the main difference consists in the calculation of the Laplacian integrals which will be calculated as smoothed sums over the neighbor particles. A column of fluid particles have been distributed along the interval $x_2 \in (0, 1)$ and no particle is set either at $x_2 = 0$ nor at $x_2 = 1$. Four rows of particles have been added to the upper and bottom parts to impose the non-slip boundary condition, where different velocities are prescribed according to the different extensions.

Using the U0M extension, the viscous shear calculated at the first and last time steps has a similar shape compared to the semi-discrete calculation presented in section V, see figure 15. Analogous results are obtained when the other extension are used, not shown here.

The global absolute error in the velocity field at the stationary state has been plotted when the extension ASM is used and the consistency of the result is clearly observed, see figure 16.

As we can see in figure 17 the U0M and the ASM extensions present similar dependence of the residual slip velocity on the smoothing length h if we compare to the continuous case studied in section V. This means that in this problem the substitution of the integrals by sums does not affect the boundary conditions excessively. It is also important to remark that when the Takeda extension is used the values of the slip velocity are more accurate compared to the other extensions (ASM and U0M), and as the others present a consistent tendency where the slip velocity tends to zero with h.

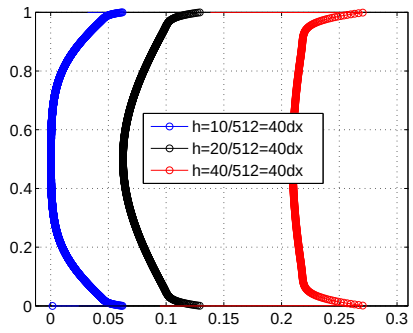

Fig. 16. Absolute error of the stationary velocity field compared with the analytical solution when the ASM approximation has been used.

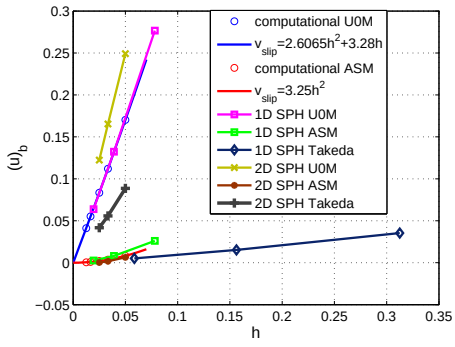

Fig. 17. Dependence on h and h^2 of the slip boundary velocity.

VII. 2D Lagrangian Discrete approximation

As SPH is well known as a Lagrangian numerical method, we tried to extend our previous ideas to this context where only the flow incompressibility and unidirectionality have been used as dominant hypothesis. In this section, the scheme used to solve the Pouseuille problem will follow a classical 2D Lagrangian SPH approximation. Comparing this procedure with the former one, in this case fluid particles fill a 2D domain $(x_1, x_2) \in [0,1]x[0,1]$ and move every time step. A periodic boundary condition is used for the inflow and outflow boundaries.

The equation (18) has been discretized in space according to the standard SPH formulation and in time by a second order Leap-Frog scheme [16]. The ratio between h and dx has been fixed for all simulations in this section $h/dx = 2$. The selection of the time step has been based on the viscous diffusion and acceleration terms [16]. Two error sources will be present in the following calculations [15]: first, due to the use of a kernel smoothing function and second, coming from the evaluation of integrals as finite sums. For the U0M and ASM extensions the boundary conditions are imposed after every predictor and corrector loop, while in the Takeda extension the boundary conditions are imposed locally in the viscous force calculation part.

In figure 17 we can appreciate how the U0M extension shows a similar tendency as in the previous implementations but the residual slip velocity has been increased by the Lagrangian movement of the particles, when the ASM extension is used this increment is almost neglegible, but the Takeda extension shows a unexpected large residual velocity that is still under interpretation.

VIII. Conclusion

The mechanism by which the non slip boundary conditions are implemented in a SPH code has been deeply understood. This paper shows how an apparently inconsistent shear force calculated at the initial step can be finally balanced by another boundary force that appears when slip velocities are present at the boundary. This convergent process allows an accurate solution of the Poiseuille problem when the smoothing length h and the ratio dx/h both tend to zero.

References

[1] H. Takeda, S. M. Miyama, and M. Sekiya, "Numerical simulation of viscous flow by Smoothed Particle Hydrodynamics," *Progress of Theoretical Physics*, vol. 92, no. 5, pp. 939–960, 1994.

[2] J. Bonet and M. Rodriguez-Paz, "Hamiltonian formulation of the variable-h sph equations," *J. Comp. Phys.*, vol. 209, pp. 541–558, 2005.

[3] J. J. Monaghan and J. B. Kajtar, "Sph boundary forces," in *4th ERCOFTAC SPHERIC workshop on SPH applications*, May 2009, pp. 216–219.

[4] T. Belytschko, Y. Krongauz, D. Organ, M. Fleming, and P. Krysl, "Meshless methods: An overview and recent developments," *Computer Methods in Applied Mechanics and Engineerings*, vol. 139, pp. 3–47, 1996.

[5] A. Souto-Iglesias, L. M. González, A. Colagrossi, and M. Antuono, "SPH no-slip BC implementation analysis at the continuous level," in *5th ERCOFTAC SPHERIC workshop on SPH applications*, 2010.

[6] J. P. Morris, P. J. Fox, and Y. Zhu, "Modeling low Reynolds number incompressible flows using SPH," *Journal of Computational Physics*, vol. 136, pp. 214–226, 1997.

[7] P. Español and M. Revenga, "Smoothed Dissipative Particle Dynamics," *Physical Review E*, vol. 67, 2003.

[8] J. J. Monaghan, "Smoothed Particle Hydrodynamic simulations of shear flow," *Monthly Notices of the Royal Astronomical Society*, vol. 365, pp. 199–213, 2005. [Online]. Available: http://dx.doi.org/10.1111/j.1365-2966.2005.09783.x

[9] A. Colagrossi and M. Landrini, "Numerical simulation of interfacial flows by smoothed particle hydrodynamics," *J. Comp. Phys.*, vol. 191, pp. 448–475, 2003.

[10] G. Liu and M. Liu, *Smoothed particle hydrodynamics. A meshfree particle method.* World Scientific Publishing Co. Pte. Ltd., 2003.

[11] F. Macià, M. Antuono, L. M. González, and A. Colagrossi, "Theoretical analysis of the no-slip boundary condition enforcement in sph methods," *Progress in Thoretical Physics*, (in press).

[12] M. Basa, N. J. Quinlan, and M. Lastiwka, "Robustness and accuracy of SPH formulations for viscous flow," *International Journal for Numerical Methods in Fluids*, vol. 60, no. 10, pp. 1127–1148, 2009.

[13] G. K. Batchelor, *Introduction to Fluid Dynamics*. Cambridge University Press, New York, 1967.

[14] D. Molteni and A. Colagrossi, "A simple procedure to improve the pressure evaluation in hydrodynamic context using the SPH," *Computer Physics Communications*, vol. 180, pp. 861–872, 2009.

[15] N. J. Quinlan, M. Lastiwka, and M. Basa, "Truncation error in mesh-free particle methods," *International Journal for Numerical Methods in Engineering*, vol. 66, no. 13, pp. 2064–2085, 2006. [Online]. Available: http://dx.doi.org/10.1002/nme.1617

[16] A. Souto-Iglesias, L. Delorme, L. Pérez Rojas, and S. Abril, "Liquid moment amplitude assesment in sloshing type problems with SPH," *Ocean Engineering*, vol. 33, pp. 11–12, 2006.